Experimental and theoretical study of valence electronic structure of tetrabromomethane by $(e, 2e)$ electron momentum spectroscopy

Zhongfeng Xu,[1] Pengfei Hu,[1] Enliang Wang,[2,*] Shenyue Xu,[1] Xing Wang,[1] Yongtao Zhao,[1] Jingkang Deng,[3] Chuangang Ning,[3] and Xueguang Ren[1,2,†]

[1]*School of Science, Xi'an Jiaotong University, 710049 Xi'an, China*

[2]*Max-Planck-Institut für Kernphysik, 69117 Heidelberg, Germany*

[3]*Department of Physics, State Key Laboratory of Low-Dimensional Quantum Physics, Tsinghua University, Beijing 100084, China*

(Received 5 March 2019; published 14 June 2019)

We report a measurement of the valence orbital momentum profiles of tetrabromomethane (CBr_4) using symmetric noncoplanar $(e, 2e)$ experiments at the impact energies of about 600 and 1200 eV. The experimental momentum profiles for the individual orbitals $5t_1$, $13t_2$, $5e$, $12t_2$, and $9a_1$ and the branching ratio of $5t_1$ to $13t_2$ and $5e$ to $13t_2$ are obtained and compared with two kinds of calculations under the plane-wave impulse approximation. One is theoretical momentum profiles that have been calculated at the equilibrium geometry, the other is those that involve vibrational effects using a thermal sampling molecular dynamics method. The calculations considering molecular vibrations are in better agreement with experiment than the equilibrium geometry calculations, indicating the important role of nuclear motions on the valence orbital electronic structures of CBr_4. The distorted-wave effects are observed in the experimental momentum profiles of $5t_1$, $5e$, and $12t_2$ which display dynamic dependencies on the impact energies. A multicenter interference or bond oscillation effect has been observed from the momentum profile ratios of $5t_1$ to $13t_2$ and $5e$ to $13t_2$ which has direct information about the bond length of a molecule.

DOI: 10.1103/PhysRevA.99.062705

I. INTRODUCTION

Electron-impact ionization $(e, 2e)$ experiments have been successfully used in the last 50 years to obtain fundamental information on the quantum few-body dynamics of the ionization process, see, e.g., [1–15], and as a direct measurement of the target initial-state one-electron wave function in momentum space, $|\psi(p)|^2$, via the so-called electron momentum spectroscopy (EMS) or the binary $(e, 2e)$ spectroscopy; see, e.g., [16–20]. For EMS, the measured $(e, 2e)$ cross section is directly proportional to the momentum-space wave function of the initial state. The unique ability of EMS to measure the electron momentum profile of an individual orbital has made it into a powerful tool for investigating the electronic structure of atoms, molecules, and condensed matter.

Tetrabromomethane, CBr_4, also known as carbon tetrabromide, is an important source of reactive halogens that have been linked to ozone depletion in both the troposphere and the stratosphere [21,22]. Furthermore, various halo-substituted compounds, in which the C-Br bond is formed, act as different classes of radiosensitizers for enhancement of the biological effectiveness in radiotherapy [23]. Such useful properties as molecular structure, chemical bonding, binding energies, and electron momentum profiles of the valence orbitals are particularly important for chemical reactivity and possibly molecular recognition [24,25]. Therefore, the investigations of the valence orbital momentum profiles by $(e, 2e)$ experiment and the associated theoretical calculations are essential for understanding the electronic and molecular structures of the reactant molecules.

Another motivation of the present work is that the electron momentum profiles of molecules are sensitive to vibration, multicenter interference, and distorted-wave effect; see, e.g., [26–42]. It is important to analyze these effects for better understanding of the experimental results. The distortion effect of the incoming and outgoing electron waves in the target and ion potentials can be analyzed experimentally as a function of the $(e, 2e)$ impact energy [34–42]. The molecule vibrational effect is related to the influence of the nuclear motion on the geometry of the molecular structure, and thus, the electron density of the individual orbitals, which can be analyzed by the molecule dynamic simulations [26–28]. The molecular orbital in momentum space can be described as a linear combination of atomic orbitals; the information about the equilibrium nuclear position $\boldsymbol{R}_j$ is presented in the phase factors of $\exp(i\boldsymbol{p}\cdot\boldsymbol{R}_j)$. As a result the momentum profile reveals an oscillation behavior, which is referred to as multicenter interference or bond oscillation effect [29–33].

In the present work, we report a combined experimental and theoretical study of EMS on CBr_4. Experimentally, the binding energy spectra (6–36 eV) and the electron momentum profiles for the valence orbitals have been measured at the projectile energies of about 600 and 1200 eV. Theoretically, a thermal sampling molecular dynamics method has been developed to consider molecular vibration in EMS. A good description of the experimental momentum profiles by considering molecular vibration indicates that nuclear dynamics can play an important role on the electronic structure of the CBr_4

*enliang.wang@mpi-hd.mpg.de
†ren@mpi-hd.mpg.de

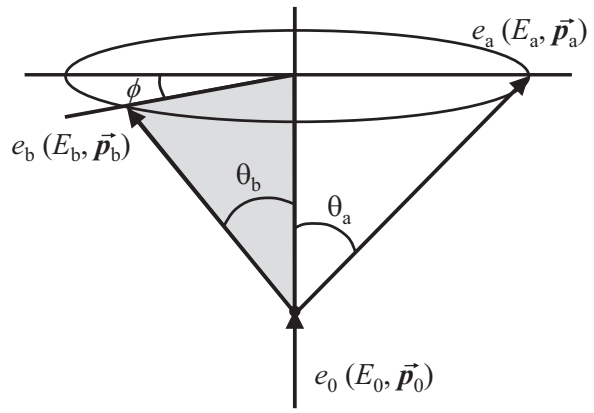

FIG. 1. Symmetric noncoplanar geometry for the present high-energy binary $(e, 2e)$ reaction.

molecule. Furthermore, we investigate the bond oscillation effect by plotting the electron momentum profile ratios of two antiphase lone pair orbitals, namely $5t_1/13t_2$ and $5e/13t_2$. The experimental ratios are well reproduced by theoretical calculations and reveal clearly an oscillation behavior.

This paper is organized as follows. After a brief description of experimental setup in Sec. II, we summarize the essential points of theoretical calculations in Sec. III. The results are presented and discussed in Sec. IV, before we finish with the conclusions in Sec. V.

II. EXPERIMENTAL SETUP

The experiment was carried out using a high-resolution and high-sensitivity electron momentum spectrometer based on a kinematically complete binary $(e, 2e)$ reaction (see Fig. 1). The details of this apparatus have been reported in previous works [43–46] and thus only a brief description will be given here. The electron beam was produced by an electron gun equipped with an oxide cathode (∼0.3 eV energy spread) and was ejected into the reaction area to collide with an effusing CBr_4 gas target. A double toroidal energy analyzer is equipped with two position- and time-sensitive detectors to detect the two outgoing electrons in coincidence. It utilizes a noncoplanar symmetric geometry (see Fig. 1), i.e., the two outgoing electrons have almost equal energies and equal polar angles ($\theta_a \approx \theta_b = 45^\circ$) with respect to the direction of the incident electron beam. A range of electron energies and out-of-plane azimuthal angles ϕ are measured in experiment. Therefore, the data acquisition efficiency is greatly increased with respect to conventional single energy and angle detection techniques.

In experiment, the binding energy ε and recoil ion momentum $\vec{q}$ can be determined by means of the energy and momentum conservation laws:

$$\varepsilon = E_0 - E_a - E_b, \tag{1}$$

$$\vec{q} = \vec{p}_0 - \vec{p}_a - \vec{p}_b. \tag{2}$$

Here E_i and $\vec{p}_i$ $(i = 0, a, b)$ are the energies and momenta of the incident, scattered, and ejected electrons, respectively. Under high-energy and high momentum-transfer conditions and the binary encounter approximation, the recoil-ion momentum $\vec{q}$ can be equal in magnitude but opposite in sign to the target bound electron momentum $\vec{p}$ [17]. The magnitude of the electron momentum p can be obtained from the measured azimuthal angle ϕ between the two outgoing electrons:

$$p = \left\{ (p_0 - \sqrt{2}p_a)^2 + 2p_a^2 \sin\left(\frac{\phi}{2}\right)^2 \right\}^{1/2}. \tag{3}$$

The binding energy resolution in the present work is about 0.7 eV, and angular resolutions are $\Delta\theta = \pm 0.6^\circ$, $\Delta\phi = \pm 0.85^\circ$ respectively, which were obtained with a calibration measurement on argon.

III. THEORETICAL CALCULATIONS

A full discussion of the EMS theory and the various approximations made to calculate $(e, 2e)$ cross sections can be found in the literature [16–20]. Within the plane-wave impulse approximation (PWIA) framework, the triple-differential cross section (TDCS) for EMS of randomly oriented molecules as function of a solid angle of two outgoing electrons, $d\Omega_a$, $d\Omega_b$, and the energy of an ejected electron, dE_b, can be expressed as

$$\begin{aligned}\sigma(\mathrm{EMS}) &= \frac{d^3\sigma}{d\Omega_a d\Omega_b dE_b} \\ &= (2\pi)^4 \frac{p_a p_b}{p_0} f_{ee} \sum_{av} |\langle pf|i\rangle|^2 \\ &= (2\pi)^4 \frac{p_a p_b}{p_0} f_{ee} M(p),\end{aligned} \tag{4}$$

where f_{ee} denotes the electron-electron collision factor which can be regarded as a constant under the present EMS experimental condition. $\sum_{av}$ means an average over initial states $|i\rangle$ and a sum over final degenerate states $|f\rangle$. $M(p)$ is the so-called structure factor which, within Born-Oppenheimer approximation (BOA), corresponds to the transition from the ν vibrational level of the initial neutral state i to the ν' vibrational level of the final ion state f. Ignoring rotational motions of molecule, the structure factor can be expressed as

$$M_{i\nu-f\nu'}(p) = \frac{1}{4\pi} \int |\langle \chi_{f\nu'}(\mathbf{Q}) | F_f(\mathbf{p};\mathbf{Q}) | \chi_{i\nu}(\mathbf{Q})\rangle|^2 d\Omega_p, \tag{5}$$

where $\chi_{i\nu}(\mathbf{Q})$ and $\chi_{f\nu'}(\mathbf{Q})$ are the vibrational wave functions of the initial and final states, respectively, with $\mathbf{Q}$ being the molecular geometry. $1/4\pi \int d\Omega_p$ represents the spherical averaging due to the random orientation of the gas-phase molecular target. $F_f(\mathbf{p};\mathbf{Q})$ is the overlap between the initial- and final-state total electronic wave function,

$$\begin{aligned}F_f(\mathbf{p};\mathbf{Q}) = \big\langle (2\pi)^{-3/2} e^{i\mathbf{p}\cdot\mathbf{r}_1} \Psi_f^{N-1}(\mathbf{r}_2, \ldots \mathbf{r}_N;\mathbf{Q}) \big| \\ \times \big| \Psi_i^N(\mathbf{r}_1, \ldots \mathbf{r}_N;\mathbf{Q}) \big\rangle,\end{aligned} \tag{6}$$

where Ψ_i^N and Ψ_f^{N-1} are the electronic wave functions of the initial neutral and final ion states, respectively. The currently achieved energy resolution of EMS does not yet allow one to resolve vibrational structures in binding-energy spectra. Thereby the final vibrational state should be summed up for all the contributions from each vibrational level ν'. Employing the closure relation of the final vibrational states,

$\sum_{v'} |\chi_{fv'}(\mathbf{Q})\rangle\langle|\chi_{fv'}(\mathbf{Q})\rangle| = 1$, the structure factor can be simplified as

$$M(p) = \int \sum_{v} P_v(T)|\chi_{iv}(\mathbf{Q})|^2 \rho(p, \mathbf{Q}) d\mathbf{Q}, \tag{7}$$

where $P_v(T)$ is the population of the initial vibrational state v at temperature T which can be determined by the Boltzmann distribution. $\rho(p, \mathbf{Q})$ denotes the spherically averaged electron momentum distribution or EMP at a fixed molecular geometry $\mathbf{Q}$ and it is given by

$$\begin{aligned}\rho(p, \mathbf{Q}) &= \frac{1}{4\pi} \int |F_f(\mathbf{p}; \mathbf{Q})|^2 d\Omega_p \\ &= \frac{1}{4\pi} S_f^{(i)}(\mathbf{Q}) \int |\varphi_f(\mathbf{p}; \mathbf{Q})|^2 d\Omega_p,\end{aligned} \tag{8}$$

in which $\varphi_f(\mathbf{p}; \mathbf{Q})$ is known as the Dyson orbital in momentum space and $S_f^{(i)}(\mathbf{Q})$ is the spectroscopic factor or pole strength describing the probability of finding a one-hole configuration $|i\rangle$ in the final state $|f\rangle$.

The TDCS for EMS of randomly oriented molecules can be simplified as

$$\sigma(\text{EMS}) \propto \int \sum_{v} P_v(T)|\chi_{iv}(\mathbf{Q})|^2 \rho(p, \mathbf{Q}) d\mathbf{Q}. \tag{9}$$

In earlier works, Watanabe *et al.* proposed the so-called harmonic analytical quantum-mechanical (HAQM) approach to study the influence of molecular vibration on EMS, which is based on a decomposition of contributions arising from each quantized vibrational eigenstate to the momentum profiles under harmonic oscillator approximation [26]. The advantage of HAQM is in reducing the computational cost compared to the calculation over the full Q space and the contributions from each normal mode can be discussed separately. Alternatively, Morini *et al.* adopted the Born-Oppenheimer molecular dynamics (BOMD) approach to perform a thermalization of molecule under certain temperature [27]. The comparison between HAQM and BOMD simulation showed that these two approaches provide an almost identical description of the vibrational effect in EMS [27,28]. In this work, a thermal sampling molecular dynamics (TSMD) method is developed to consider the vibrational effects in EMS. The influence of thermal energy to molecular geometry is analyzed and sampled under target temperature T using the quasiclassical fixed normal-mode sampling method [47]. T is about 300 K (room temperature) in the present experiments. The populations of the vibrational states are sampled using Boltzmann distribution. Such a procedure is usually referred to as a thermal sampling process, which simulates the molecular rotation vibration under certain temperatures. The TDCS can be further expressed as

$$\sigma(\text{EMS}) \propto \frac{1}{N} \sum_{j}^{N} \sum_{v} P_v(T)|\chi_{iv}(\mathbf{Q}_j)|^2 \rho(p, \mathbf{Q}_j) \Delta\mathbf{Q}_j, \tag{10}$$

where $N = 1000$ in this work denotes the number of molecular geometries obtained in the thermal sampling process which was performed by density-functional theory (DFT) along with the Becke three-parameters Lee-Yang-Parr (B3LYP) functional method [48,49] using the cc-pVDZ basis set. The momentum profiles at fixed geometry were calculated at the B3LYP/aug-cc-pVTZ level. All of the calculations were carried out using the GAUSSIAN package [47]. To compare with experiment, the theoretical momentum profiles have been convoluted with the experimental resolutions.

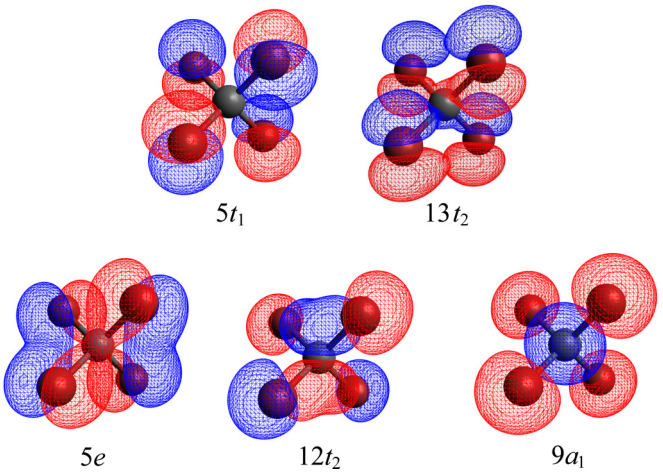

FIG. 2. Maps of the outer-valence molecular orbitals of CBr_4.

IV. RESULTS AND DISCUSSIONS

CBr_4 belongs to T_d symmetry and its ground-state electronic configuration can be described as

$$(\text{core})^{114} \underbrace{(8a_1)^2(11t_2)^6}_{\text{Inner valence}} \underbrace{(9a_1)^2(12t_2)^6(5e)^4(13t_2)^6(5t_1)^6}_{\text{Outer valence}}.$$

The position space molecular orbital maps for the outer valence orbitals of CBr_4 are shown in Fig. 2. Here, the electron density is mainly located at four Br atoms except for the $9a_1$ orbital. The $5t_1$, $13t_2$, $5e$ orbitals are essentially due to lone-pair electrons of the Br $5p$ nonbonding atomic orbitals; they may give prominent oscillatory structures due to the multicenter interference effect [29–33].

A. Binding-energy spectra

Figure 3 presents the experimental binding-energy spectra of CBr_4. The binding-energy spectra at different ϕ angles can be obtained simultaneously in the experiment. From the angle-energy density map displayed in Fig. 3(a), the basic features of EMS for each orbital can be seen directly. Density minima are observed for each orbital at the azimuthal angle $\phi = 0°$, i.e., the momentum origin ($p \sim 0$ a.u.), except for the $9a_1$ orbital. The $9a_1$ orbital shows a sp-type feature because the C $2s$ state contributes to the $9a_1$ orbital while the others contain mainly the Br $5p$ state. The binding-energy spectrum in the bottom panel of Fig. 3 was obtained by summing all the energy spectra for different ϕ angles. To obtain the experimental momentum profile for each orbital, the binding-energy spectra at the different ϕ angles were fitted with the multiple Gaussian functions. The peak centers were determined through high-resolution photoelectron spectroscopy (PES) [50], and the widths were determined by combining the experimental energy resolution and the vibrational broadening on PES. The experimental momentum profiles were obtained by

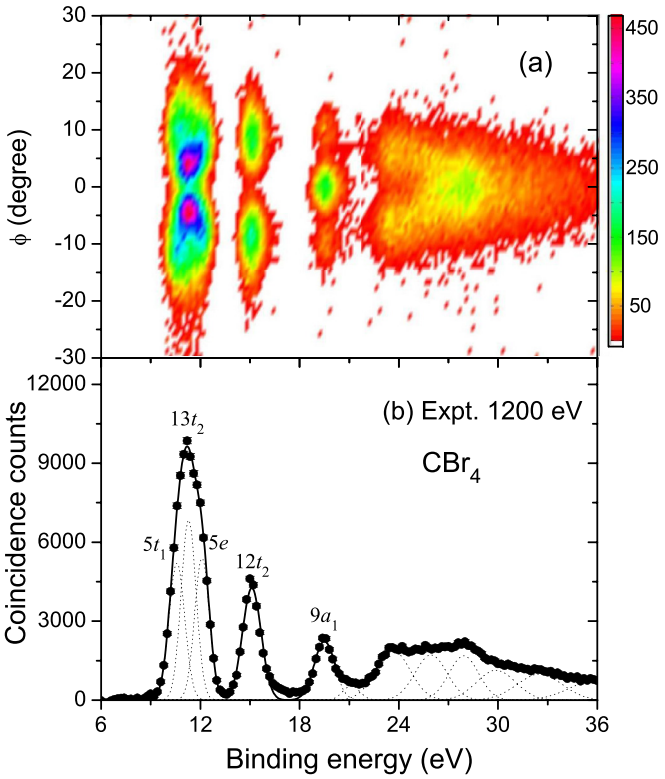

FIG. 3. (a) Experimental momentum-energy density map of CBr_4 and (b) binding-energy spectrum summed over all azimuthal angles ϕ obtained at the impact energy of 1200 eV plus binding energies. The dashed lines represent Gaussian fits to the individual peaks and the solid curve is the summed fit. The labels are the outer-valence orbital assignments.

fitting the intensity for each state plotted as a function of the momentum p.

The measured binding energies of this work and early published PES data and the calculated values using DFT and outer valence Green-function (OVGF) methods are compared in Table I. The OVGF calculated binding energies of outer valence orbitals are closer to the EMS and PES measured values than the DFT calculations.

TABLE I. Measured and calculated binding energies (eV) for the outer valence orbitals of CBr_4.

Orbital	PES[a]	EMS	B3LYP/ aug-cc-pVTZ	OVGF/ aug-cc-pVTZ
	10.40			
$5t_1$	10.49	10.58	8.04	11.26
	10.75			
	11.05			
$13t_2$	11.23	11.29	8.86	11.95
	11.69			
$5e$	12.06	12.10	9.52	13.04
$12t_2$	15.04	15.11	12.70	16.25
$9a_1$	19.48	19.50	16.58	21.65

[a]Reference [50].

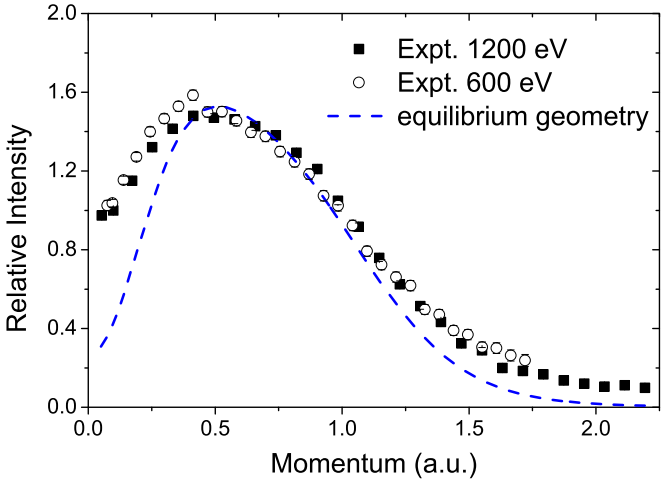

FIG. 4. Measured and calculated momentum profiles for the sum of $5t_1 + 13t_2 + 5e + 12t_2 + 9a_1$ orbitals of CBr_4 at the impact energies of 600 and 1200 eV. The dashed curve is the calculations with DFT-B3LYP/aug-cc-pVTZ method at the equilibrium geometry of CBr_4.

To compare the experimental momentum profiles with theory, a normalization procedure is needed because the experimental intensity is on a relative scale. A global normalization factor was determined by fitting the summed outer valence momentum profiles in Fig. 3 to the corresponding calculations, i.e., $5t_1 + 13t_2 + 5e + 12t_2 + 9a_1$, and then this factor was used to normalize the experimental data for each orbital. As shown in Fig. 4, the experimental results for two different impact energies agree well with each other for the momentum region $p > 0.5$ a.u.. Therefore the data in this region were used to determine the normalization factor, which was obtained by normalizing the experimental data to the calculation at p about 0.8 a.u.

B. Electron momentum profiles

The momentum profiles for the individual $5t_1$, $13t_2$, $5e$, $12t_2$, and $9a_1$ orbitals of CBr_4 are presented in Fig. 5. The $5t_1$, $13t_2$, and $5e$ orbitals are mainly composed of the $5p$ lone pair electron of Br atoms. In principle, these orbitals display a p-type feature on the momentum profiles. The results for $5t_1$ and $5e$ show p-type features with a maximum located at about 0.8 and 0.6 a.u., respectively. For $13t_2$, a double p-type feature is observed with two maxima located at $p \sim 0.35$ and 1.0 a.u. The differences among these three orbitals originate from the different orientations of the $5p$ lone pair orbital of Br. As shown in Fig. 2, two antiparallel $5p$ lone pairs contribute to the orbital of $5t_1$ from the left or right sides two bromines. The orbital of $5e$ is attributed to the top or bottom sides two bromines. For these two orbitals only a small phase shift will be present on their p-type momentum profiles, while for the orbital of $13t_2$ all four bromines with almost parallel lone pairs contribute to its orbital, which shows an antiphase feature of momentum profile as can be seen in Fig. 5(b). The $12t_2$ and $9a$ orbitals correspond to the covalent bond between C and Br atoms. A p-type momentum profile is displayed with a maximum located at 0.7 a.u. while a sp-type feature is

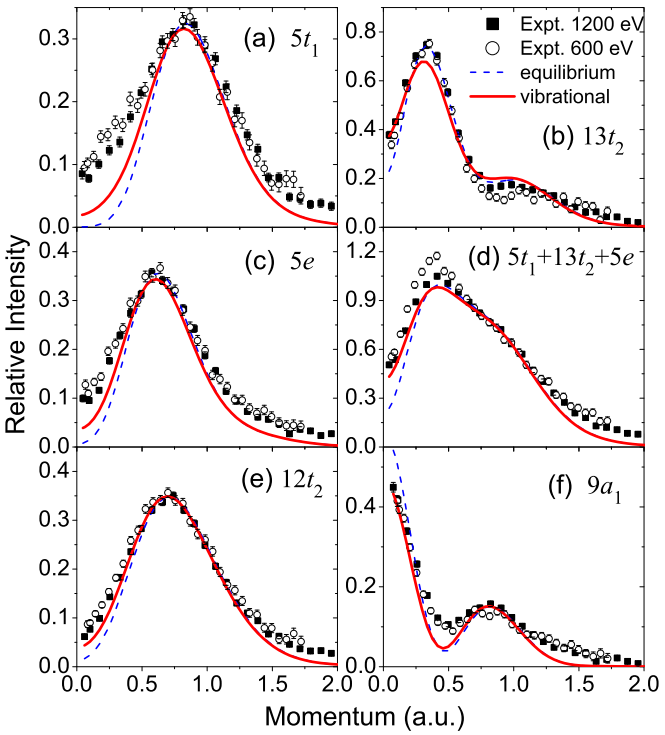

FIG. 5. Measured and calculated electron momentum profiles for the outer valence orbitals of CBr_4 at the impact energies of 600 and 1200 eV. The dashed curves are calculations at the equilibrium geometry of CBr_4. The molecule vibrational calculations are shown by the solid curves.

observed for $9a$ with two maxima located at the momentum origin and 0.8 a.u., respectively.

The experimental momentum profiles are compared with two kinds of calculations in Figs. 5(a)–5(f) for the states $5t_1$, $13t_2$, $5e$, $5t_1 + 13t_2 + 5e$, $12t_2$, and $9a_1$, respectively. One is theoretical momentum profiles (dashed lines) that have been calculated at the equilibrium geometry while vibrational effects were not taken into account. The other is those that involve vibrational effects (solid lines). The experimental data are generally well described by both calculations in the high-momentum range ($p > 0.7$ a.u.). However at low momenta ($p < 0.7$ a.u.) there is an unexpected higher intensity observed for the states $5t_1$, $5e$, and $12t_2$ compared to the equilibrium geometry calculations, which has been called the "turn-up" effect in EMS [34–42]. Further calculations considering molecular vibration show better agreement with the experimental data than the equilibrium geometry calculations. It can be seen in Fig. 5(d) that the summed $5t_1 + 13t_2 + 5e$ momentum profile is rather well reproduced by the vibrational calculations. It is shown from comparison between experiment and theory that molecular vibration is partly (~50%) responsible for the observed turn-up effect of the $5t_1$, $5e$, and $12t_2$ orbital momentum profiles. Another possible reason for the observed higher intensity at low momenta is the distortion effect of the incoming and outgoing electron waves in the target and the ion potentials, since the size of the effect decreases with increasing impact energy [34]. For $13t_2$ and $9a_1$ orbitals, the experimental momentum profiles show higher intensity for $13t_2$ and lower intensity for $9a_1$ compared to the equilibrium

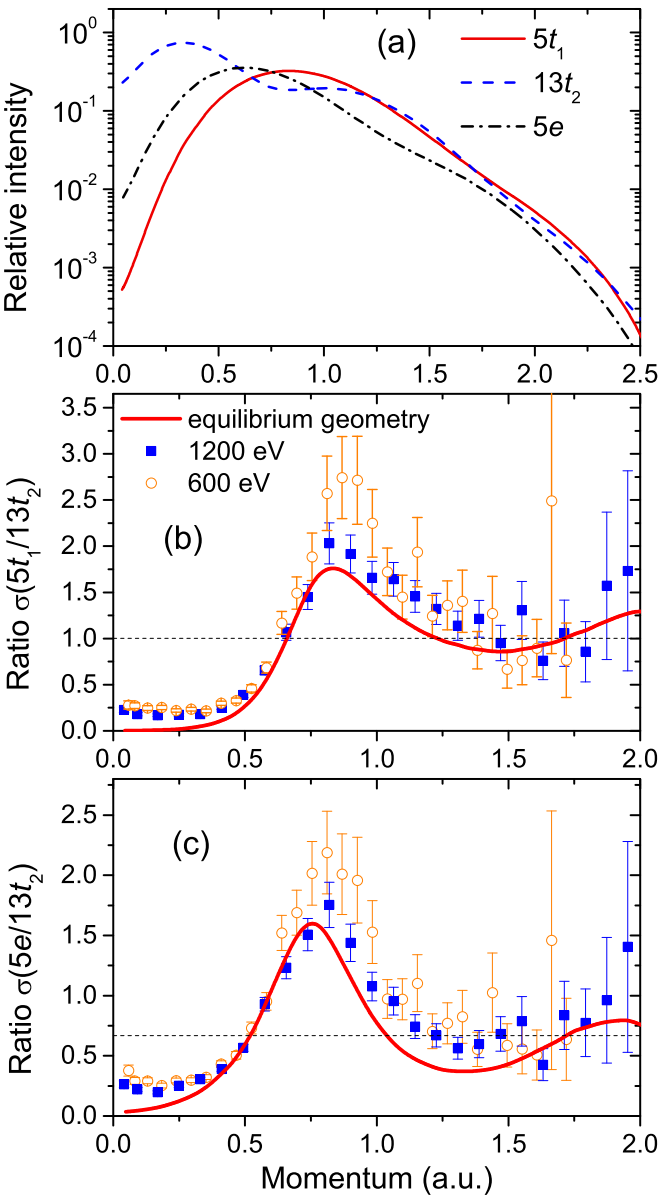

FIG. 6. The momentum profiles for $5t_1$, $13t_2$, and $5e$ orbitals in logarithmic scale (a), and the momentum profile ratios for $5t_1/13t_2$ (b) and $5e/13t_2$ (c).

geometry calculations. The vibrational effect calculations are in much better agreement with the experimental data than the equilibrium geometry calculations especially at low momenta ($p < 0.25$ a.u.). The experimental results at the impact energies of 600 and 1200 eV are almost identical to each other, indicating the influence of the distorted-wave effect to be quite small for these two orbitals.

C. Bond oscillation effect

As discussed above, $5t_1$, $13t_2$, and $5e$ are mainly composed of Br $5p$ lone pair orbitals which are expected to observe bond oscillation effects [29–33]. Here, we investigate the bond oscillation effect by plotting the ratio of two orbitals with antiphase feature in momentum profiles, i.e., $5t_1/13t_2$ and $5e/13t_2$. This provides an alternative way to extract the

multicenter interference pattern in which the oscillation structures can be magnified [32].

The momentum profiles in the logarithmic scale are presented in Fig. 6(a) where the antiphase features are clearly visible for $5t_1/13t_2$ and $5e/13t_2$. The experimental ratios at the impact energies of 600 and 1200 eV are presented in Figs. 6(b) and 6(c) for $5t_1/13t_2$ and $5e/13t_2$, respectively. Also included in the figures are the equilibrium geometry calculations. The momentum profile ratios exhibit significant oscillations around constant values which is the distinct evidence of the multicenter interference effect. The constant ratios are determined by the number of electrons occupied in each molecular orbital, i.e., 1 for $5t_1/13t_2$ and $2/3$ for $5e/13t_2$. The experimental ratios are in good agreement with theoretical calculations both in magnitudes and peak positions. The resulting R_{BrBr} value of 3.21 Å has been found to be in good agreement with 3.15 Å reported by electron diffraction [51].

V. CONCLUSIONS

We have reported a combined experimental and theoretical study of the valence electronic structure of tetrabromomethane (CBr_4) by electron momentum spectroscopy (EMS). The binding-energy spectra were measured with resolution of $\Delta\varepsilon \sim 0.7$ eV for the energy range from 6 to 36 eV. The valence orbital momentum profiles were measured at the impact energies of about 600 and 1200 eV using a high-sensitivity binary $(e, 2e)$ spectrometer. The experimental momentum profiles for the individual $5t_1$, $13t_2$, $5e$, $12t_2$, and $9a_1$ orbitals were compared with theoretical momentum profiles calculated at the equilibrium geometry of CBr_4 and also using the thermal sampling molecular dynamics (TSMD) method in which 1000 thermally sampled geometries were involved to consider the molecule vibrational effect.

It was found that the experimental momentum profiles are generally well described by both calculations in the high-momentum range ($p > 0.7$ a.u.). However at low momenta ($p < 0.7$ a.u.) there is an unexpected higher intensity observed for the $5t_1$, $5e$, and $12t_2$ orbitals compared to theoretical results at the equilibrium geometry. Calculations considering molecular vibration indicate that the higher intensity at the low momenta can be partly, i.e., roughly 50%, attributed to vibrational effects. This indicates the important role of nuclear motions on the valence orbital electronic structure of CBr_4. Another possible reason for the observed higher intensity at low momenta is the distortion effect of the incoming and outgoing electron waves in the nuclear potential, since the size of the effect decreases with increasing impact energy. Finally, we investigate the bond oscillation effect in the lone pair orbitals of $5t_1$, $13t_2$, and $5e$ using the electron momentum profile ratios for $5t_1$ to $13t_2$ and $5e$ to $13t_2$. The experimental ratios are in good agreement with theoretical calculations and reveal clearly the oscillatory structures. The resulting internuclear distance of 3.21 Å between the Br atoms is consistent with the value reported by electron-diffraction experiment.

ACKNOWLEDGMENTS

This work was supported by the National Natural Science Foundation of China under Grants No. 11774281, No. 11875219, and No. U1532263, Science Challenge Project No. TZ2016005. E.W. acknowledges a fellowship from the Alexander von Humboldt Foundation.

[1] K. Bartschat, J. Phys. B **51**, 132001 (2018).
[2] I. Bray, D. Fursa, A. Kadyrov, A. Stelbovics, A. Kheifets, and A. Mukhamedzhanov, Phys. Rep. **520**, 135 (2012).
[3] X. Ren, S. Amami, O. Zatsarinny, T. Pflüger, M. Weyland, W. Y. Baek, H. Rabus, K. Bartschat, D. Madison, and A. Dorn, Phys. Rev. A **91**, 032707 (2015).
[4] T. N. Resigno, M. Baertschy, W. A. Isaacs, and C. W. McCurdy, Science **286**, 2474 (1999).
[5] O. Al-Hagan, C. Kaiser, A. J. Murray, and D. Madison, Nat. Phys. **5**, 59 (2009).
[6] T. Pflüger, O. Zatsarinny, K. Bartschat, A. Senftleben, X. Ren, J. Ullrich, and A. Dorn, Phys. Rev. Lett. **110**, 153202 (2013).
[7] D. B. Jones, E. Ali, C. G. Ning, J. Colgan, O. Ingólfsson, D. H. Madison, and M. J. Brunger, J. Chem. Phys. **145**, 164306 (2016).
[8] X. Ren, T. Pflüger, J. Ullrich, O. Zatsarinny, K. Bartschat, D. H. Madison, and A. Dorn, Phys. Rev. A **85**, 032702 (2012).
[9] C. M. Granados-Castro and L. U. Ancarani, Eur. Phys. J. D **71**, 65 (2017).
[10] X. G. Ren, C. G. Ning, J. K. Deng, G. L. Su, S. F. Zhang, Y. R. Huang, and G. Q. Li, Phys. Rev. A **72**, 042718 (2005).
[11] J. Colgan, M. S. Pindzola, F. Robicheaux, C. Kaiser, A. J. Murray, and D. H. Madison, Phys. Rev. Lett. **101**, 233201 (2008).
[12] X. Ren, S. Amami, O. Zatsarinny, T. Pflüger, M. Weyland, A. Dorn, D. Madison, and K. Bartschat, Phys. Rev. A **93**, 062704 (2016).
[13] A. Naja, E. M. Staicu-Casagrande, X. G. Ren, F. Catoire, A. Lahmam-Bennani, C. D. Cappello, and C. T. Whelan, J. Phys. B **40**, 2871 (2007).
[14] X. Ren, A. Senftleben, T. Pflüger, A. Dorn, K. Bartschat, and J. Ullrich, Phys. Rev. A **83**, 052714 (2011).
[15] X. Li, X. Ren, K. Hossen, E. Wang, X. Chen, and A. Dorn, Phys. Rev. A **97**, 022706 (2018).
[16] C. E. Brion, Int. J. Quantum Chem. **29**, 1397 (1986).
[17] I. E. McCarthy and E. Weigold, Rep. Prog. Phys. **54**, 789 (1991).
[18] M. A. Coplan, J. H. Moore, and J. P. Doering, Rev. Mod. Phys. **66**, 985 (1994).
[19] M. Vos and I. E. McCarthy, Rev. Mod. Phys. **67**, 713 (1995).
[20] M. Takahashi, Bull. Chem. Soc. Jpn. **82**, 751 (2009).
[21] J. R. Greene, J. S. Francisco, D. Xu, J. Huang, and W. M. Jackson, J. Chem. Phys. **125**, 133311 (2006).

[22] Q. Kong, M. Wulff, J. H. Lee, S. Bratos, and H. Ihee, J. Am. Chem. Soc. **129**, 13584 (2007).
[23] M. C. Castrovilli, P. Markush, P. Bolognesi, P. Rousseau, S. Maclot, A. Cartoni, R. Delaunay, A. Domaracka, J. Kočišek, B. A. Huber, and L. Avaldi, Phys. Chem. Chem. Phys. **19**, 19807 (2017).
[24] C. Brion, G. Cooper, Y. Zheng, I. Litvinyuk, and I. McCarthy, Chem. Phys. **270**, 13 (2001).
[25] K. Fukui, Angew. Chem., Int. Ed. Engl. **21**, 801 (1982).
[26] N. Watanabe, M. Yamazaki, and M. Takahashi, J. Chem. Phys. **137**, 114301 (2012).
[27] F. Morini, M. S. Deleuze, N. Watanabe, and M. Takahashi, J. Chem. Phys. **142**, 094308 (2015).
[28] Y. Tang, X. Shan, J. Yang, S. Niu, Z. Zhang, N. Watanabe, M. Yamazaki, M. Takahashi, and X. Chen, J. Phys. Chem. A **120**, 6855 (2016).
[29] N. Watanabe, X. J. Chen, and M. Takahashi, Phys. Rev. Lett. **108**, 173201 (2012).
[30] Z. Zhang, X. Shan, T. Wang, E. Wang, and X. Chen, Phys. Rev. Lett. **112**, 023204 (2014).
[31] M. Yamazaki, H. Satoh, N. Watanabe, D. B. Jones, and M. Takahashi, Phys. Rev. A **90**, 052711 (2014).
[32] E. Wang, X. Shan, Q. Tian, J. Yang, M. Gong, Y. Tang, S. Niu, and X. Chen, Sci. Rep. **6**, 39351 (2016).
[33] N. Watanabe, K. Katafuchi, M. Yamazaki, and M. Takahashi, Eur. Phys. J. D **70**, 268 (2016).
[34] C. E. Brion, Y. Zheng, J. Rolke, J. J. Neville, I. E. McCarthy, and J. Wang, J. Phys. B **31**, L223 (1998).
[35] X. Ren, C. Ning, J. Deng, S. Zhang, G. Su, F. Huang, and G. Li, Chem. Phys. Lett. **404**, 279 (2005).
[36] X. G. Ren, C. G. Ning, J. K. Deng, S. F. Zhang, G. L. Su, F. Huang, and G. Q. Li, Phys. Rev. Lett. **94**, 163201 (2005).
[37] C. G. Ning, X. G. Ren, J. K. Deng, G. L. Su, S. F. Zhang, and G. Q. Li, Phys. Rev. A **73**, 022704 (2006).
[38] X. Ren, C. Ning, J. Deng, S. Zhang, G. Su, Y. Huang, and G. Li, J. Electron Spectrosc. Relat. Phenom. **151**, 92 (2006).
[39] X. G. Ren, C. G. Ning, J. K. Deng, G. L. Su, S. F. Zhang, and Y. R. Huang, Phys. Rev. A **73**, 042714 (2006).
[40] C. D. Cappello, F. Menas, S. Houamer, Y. V. Popov, and A. C. Roy, J. Phys. B **48**, 205201 (2015).
[41] X. Wang, S. Xu, C. Ning, O. Al-Hagan, P. Hu, Y. Zhao, Z. Xu, J. Deng, E. Wang, X. Ren, A. Dorn, and D. Madison, Phys. Rev. A **97**, 062704 (2018).
[42] S. Xu, C. Ma, E. Wang, P. Hu, X. Wang, Y. Zhao, Z. Xu, J. Deng, C. Ning, A. Dorn, and X. Ren, Phys. Rev. A **99**, 022705 (2019).
[43] X. G. Ren, C. G. Ning, J. K. Deng, S. F. Zhang, G. L. Su, F. Huang, and G. Q. Li, Rev. Sci. Instrum. **76**, 063103 (2005).
[44] X.-G. Ren, C.-G. Ning, J.-K. Deng, S.-F. Zhang, G.-L. Su, B. Li, and X.-J. Chen, Chin. Phys. Lett. **22**, 1382 (2005).
[45] C.-G. Ning, S.-F. Zhang, J.-K. Deng, K. Liu, Y.-R. Huang, and Z.-H. Luo, Chin. Phys. B **17**, 1729 (2008).
[46] C. G. Ning, J. K. Deng, G. L. Su, H. Zhou, and X. G. Ren, Rev. Sci. Instrum. **75**, 3062 (2004).
[47] M. F. Frisch, G. W. Trucks, H. B. Schlegel *et al.*, Gaussian03 Revision E.01, Gaussian Inc. Wallingford CT, 2004.
[48] A. D. Becke, J. Chem. Phys. **98**, 5648 (1993).
[49] C. Lee, W. Yang, and R. G. Parr, Phys. Rev. B **37**, 785 (1988).
[50] J. C. Green, M. L. H. Green, P. J. Joachim, A. F. Orchard, D. W. Turner, W. C. Price, and D. W. Turner, Philos. Trans. R. Soc. London A **268**, 111 (1970).
[51] Y. He, J. Zhang, and W. Kong, J. Chem. Phys. **145**, 034307 (2016).